

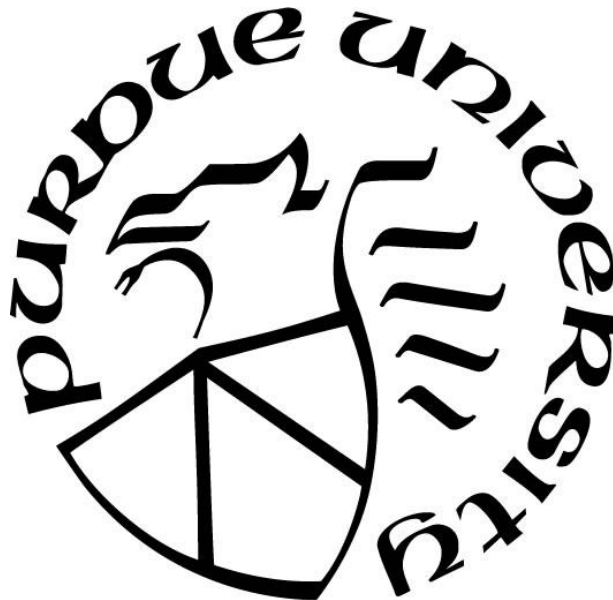
**PREDICTION OF DELIVERED AND IDEAL SPECIFIC IMPULSE USING
RANDOM FOREST MODELS AND PARSIMONOUS NEURAL
NETWORKS**

by
Peter Joseph Salek

A Thesis

*Submitted to the Faculty of Purdue University
In Partial Fulfillment of the Requirements for the degree of*

Master of Science in Aeronautics and Astronautics



School of Aeronautics and Astronautics
West Lafayette, Indiana
May 2022

**THE PURDUE UNIVERSITY GRADUATE SCHOOL
STATEMENT OF COMMITTEE APPROVAL**

Dr. Alejandro Strachan, Co-Chair

School of Materials Engineering

Dr. Steven Son, Co-Chair

School of Mechanical Engineering

Dr. Weinong Chen

School of Aeronautics and Astronautics

Approved by:

Dr. Gregory A. Blaisdell

Dedicated to my family, friends, and all who supported me along the way.

ACKNOWLEDGMENTS

I would like to thank everyone who supported me and made this work possible. I would first like to thank my advisor, Dr. Alejandro Strachan, for his guidance and insights. I am extremely thankful for the time and effort he provided. His passion for research and sharing his knowledge is truly inspiring.

I would also like to thank the members of the Strachan group and the members of the DARPA RIDE project. The feedback and suggestions during weekly meetings and casual conversations were critical to advancing my work. I always felt comfortable asking anyone questions on problems I was having with my research and am extremely grateful for this. The enthusiasm to help each other succeed and work together as a group to solve difficult problems was way beyond any of my expectations.

Lastly, I would like to thank my parents and my brothers, Walter, Jackie, Nick, and Will, for their unconditional love and support. I would also like to thank my committee members, Dr. Steven Son and Dr. Weinong Chen,

"This research was developed with funding from the Defense Advanced Research Projects Agency (DARPA). The views, opinions and/or findings expressed are those of the author and should not be interpreted as representing the official views or policies of the Department of Defense or the U.S. Government."

TABLE OF CONTENTS

LIST OF TABLES	7
LIST OF FIGURES	8
LIST OF EQUATIONS	9
ABSTRACT.....	10
1. INTRODUCTION	11
1.1 Principles of Rockets	12
1.2 Obtaining Experimental Data	15
1.3 Applying Data Science Tools and Machine Learning	16
2. METHODS	17
2.1.1 Delivered Specific Impulse Data.....	17
2.1.2 Ideal Specific Impulse Data.....	18
2.2 Random Forest Models	19
2.3 Parsimonious Neural Networks and Genetic Algorithms.....	19
3. DELIVERED SPECIFIC IMPULSE.....	22
4. IDEAL SPECIFIC IMPULSE	28
4.1 KJ Inputs	28
4.2 CHNO Inputs	29
5. CONCLUSION.....	32
5.1 Delivered Specific Impulse.....	32
5.2 Ideal Specific Impulse.....	32
APPENDIX A. DELIVERED SPECIFIC IMPULSE DATA[2,25,31,32]	33
APPENDIX B. IDEAL SPECIFIC IMPULSE DATA[16]	36
REFERENCES	45

LIST OF TABLES

Table 2.1. Sample of open literature data collected for the delivered specific impulse models...	17
Table 2.2. A sample of the data used for the ideal specific impulse models.	19
Table 3.1. Inputs for Models 1 and 2	22
Table 3.2. Range of testing properties and some of the training data used.	23
Table 3.3. Training data points values.	25
Table 3.4. Model 3 and 4 inputs.	27

LIST OF FIGURES

Figure 1.1. The figure above depicts how conservation of momentum is applied to rockets. [17]	12
Figure 1.2. The figure depicts a cross section of a solid rocket motor. [18].....	13
Figure 1.3. The above image depicts a converging diverging nozzle. [19].....	14
Figure 2.1. This figure depicts certain parts of a rocket engine and nozzle that are in the data columns. [26]	18
Figure 3.1. Parity plot for model 1 and 2.....	23
Figure 3.2. This figure depicts model 1s prediction of a range of ideal specific impulse.	24
Figure 3.3. This figure depicts model 2’s prediction for a range of AP and AN over a variety of motor configurations.	26
Figure 3.4. Parity plot for model 3 and model 4.....	27
Figure 4.1. Pareto Front: KJ Inputs.....	28
Figure 4.2. Pareto Front: KJ Inputs Normalized.....	29
Figure 4.3. Pareto Front: CHNO Inputs.....	30
Figure 4.4. Pareto Front: CHNO Inputs zoomed in around MLRA	30

LIST OF EQUATIONS

Equation 1.1. Specific Impulse	13
Equation 1.2. Example chemical equation.....	13
Equation 1.3. C* relation to propellant properties	14
Equation 1.4. Area Mach Relation.....	15
Equation 1.5. Isentropic Pressure relations.....	15
Equation 2.1. Activation function calculation.	20
Equation 2.2. Custom multiply activation function.....	20
Equation 2.3. Even root activation function.	20
Equation 2.4. Constraint activation function.	20
Equation 2.5. Objective function of genetic algorithm.....	21
Equation 3.1. Solids loading relationship.	25

ABSTRACT

Development of complex aerospace systems often takes decades of research and testing. High performing propellants are important to the success of rocket propulsion systems. Development and testing of new propellants can be expensive and dangerous. Full scale tests are often required to understand the performance of new propellants. Many industries have started using data science tools to learn from previous work and conduct smarter tests. Material scientists have started using these tools to speed up the development of new materials. These data science tools can be used to speed up the development and design better propellants. I approach the development of new solid propellants through two steps: Prediction of delivered performance from available literature tests, prediction of ideal performance using physics-based models. Random Forest models are used to correlate the ideal performance to delivered performance of a propellant based on the composition and motor properties. I use Parsimonious Neural Networks (PNNs) to learn interpretable models for the ideal performance of propellants. I find that the available open literature data is too biased for the models to learn from and discover families of interpretable models to predict the ideal performance of propellants.

1. INTRODUCTION

Aerospace systems have accomplished extraordinary tasks throughout their existence. We've sent humans to The Moon during the Apollo program and sent satellites out of our galaxy in the voyager missions. These systems took decades of research and testing to successfully launch. As we look to expand what aerospace systems can accomplish, we need to be smarter in the way we develop new systems. Using data science tools, researchers can learn more from previous work to guide advances in new technologies. Designing new propellant formulations is an important part of designing better aerospace systems.

Composite solid rocket propellants have been used since the days of the Apollo missions and are often made of ingredients such as HTPB, Ammonium Perchlorate, Ammonium Nitrate, Aluminum, Iron Oxide. [1] Studies have been conducted to understand the effect of weight percentages, particle size, solids loading, metalized vs non-metalized, casting procedures, and motor configurations on performance. [2–5] Variations in these can result in changes in both the ideal and delivered performance of the propellant. Models capable of predicting the performance of propellants can accelerate the development of new propellants. This is especially important in the field of energetics where experiments are time consuming, expensive, and dangerous.

Modern methods use complex thermochemical codes such as NASA CEA and Cheetah, that with a database of composition and heats of formation, can be used to predict ideal performance parameters for a fixed motor geometry and operating conditions. [6] For a new potential propellant, if an experimental test has not been conducted, the heat of formation can be estimated from expensive quantum chemistry calculations.

Development of new energetic materials often take decades of research and testing. [7] Data science tools have been used to rapidly decrease the development time of new materials. Recent studies have shown that more and more studies are applying data science tools to archival data. Archival data is poorly report and often researchers disagree on what is important to report in published data. [8,9] This issue is being open addressed within the field and researchers are actively working to make data more available to data scientists. [10,11] With researchers making data more available, progress has been made in the field of materials in battery applications and high-temperature oxides. [12,13] The field of energetics have also been successfully using available data to build models to predict detonation velocity and pressures of explosives. [14]

Recent efforts have been made to develop models capable of predicting the ideal specific impulse of CHNO propellants using the Kamlet-Jacobs decomposition assumption. [15] The work develops a simple expression, using the heat of combustion and the number of grams per gaseous mole, to predict the ideal specific impulse of 165 different propellants. [16] This model assumes a motor operating pressure of 1000 psi and a nozzle pressure ratio of 68.9. Motor operating conditions and motor geometry have a great effect on both the ideal and delivered performance of the propellant. Understanding how rockets generate thrust is important to understanding potential area of loss within propellant performances.

1.1 Principles of Rockets

The foundation of rocket propulsion systems are built around Isaac Newton’s third law of motion. Newton states, “For every action, there is an equal and opposite reaction.” Propellants, the fuel of rocket propulsion, is combusted and accelerated out the nozzle of the rocket. The highspeed exhaust gases are ejected out of the nozzle and the rocket feels the reaction force called thrust. The law of conservation of momentum states that the momentum of a system must always be conserved. When the high velocity low mass exhaust is moving away from the rocket, the high mass rocket must move in the opposite direction at a slower speed to conserve the momentum of our rocket system. This allows rocket propulsion system to be effective in the vacuum of space and within the atmosphere.

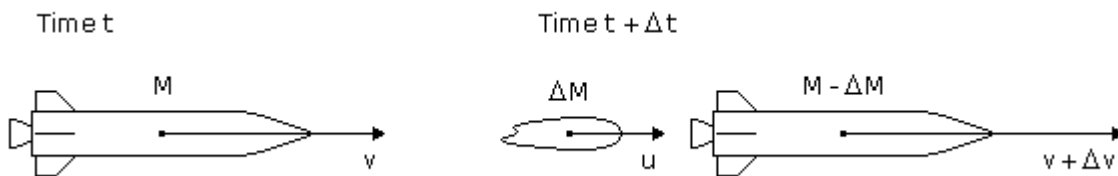


Figure 1.1. The figure above depicts how conservation of momentum is applied to rockets. [17]

Since the goal of rocket engines is to generate thrust, efficiencies of rocket engines are how effectively an engine and fuel combination creates thrust per amount of fuel needed. This is known as the specific impulse, or the amount of thrust generated per unit mass flow. Specific impulse is affected by the characteristics of the propellant, the chamber pressure of the engine, and the

expansion ratio of the nozzle. Ideal specific impulse is the maximum efficiency a combination of these parameters could achieve. The ideal specific impulse assumes complete combustion and zero losses within the rocket engine and nozzle. The delivered specific impulse is the actual realized efficiency of a rocket engine operating with real conditions. Real rocket engines experience a specific impulse efficiency which accounts for all the losses within the combustion process and the nozzle. To separate some areas of the rocket, we will look at the rocket in two sections: The combustor and the nozzle.

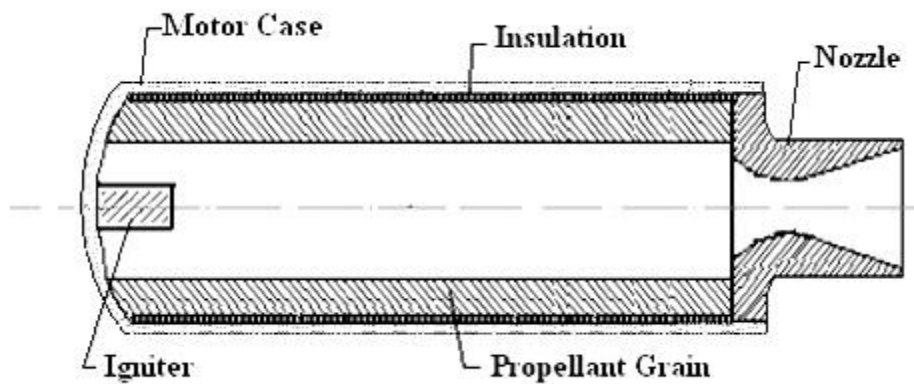
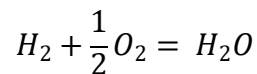


Figure 1.2. The figure depicts a cross section of a solid rocket motor. [18]

$$I_{sp} = \frac{F}{\dot{m}}$$

Equation 1.1. Specific Impulse

In the rocket combustor, fuel and oxidizer are mixed and burned at a high pressure. The combustor provides the hot gases to the nozzle that will generate the thrust discussed above. Fuel and oxidizers burned together can be represented in a chemical equation to combust into its products.



Equation 1.2. Example chemical equation

Complete combustion occurs when all the fuel has been fully oxidized and the most energy has been released from the combustion process. In real rocket combustors, incomplete combustion will occur and some of the products exiting the combustor will not be fully oxidized. Products that are not fully oxidized reduce the efficiency of the combustion process. Combustion efficiency is measured by a term called the characteristic velocity. The ideal characteristic velocity represents the max efficiency of a propellant when it is fully combusted. Incomplete combustion results in a loss of the c^* realized by the rocket engine.

$$c^* = \frac{P_c A_t}{\dot{m}} = \sqrt{\frac{R_u T_c}{\gamma MW}} \left(\frac{2}{\gamma + 1} \right)^{\frac{\gamma + 1}{2(\gamma - 1)}}$$

Equation 1.3. C^* relation to propellant properties

Rocket nozzles use the high-pressure combustion products from the combustor and accelerate the gases away from the rocket. A converging-diverging nozzle is used to expand the high-pressure gases and accelerate the flow out the end of the rocket engine.

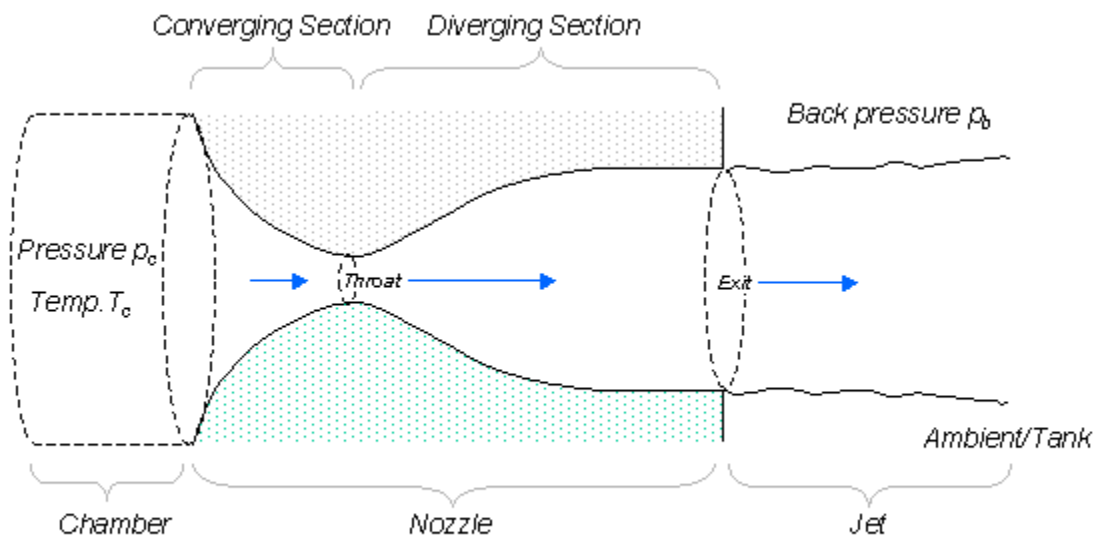


Figure 1. Converging Diverging Nozzle Configuration

Figure 1.3. The above image depicts a converging diverging nozzle. [19]

The flow will travel from the combustor, accelerated through the converging section, be choked at the throat, and accelerated again out the diverging section of the nozzle. The exhaust products accelerate through the converging-diverging section of the nozzle as a function of the area ratio and the ratio of specific heats.

$$\frac{A}{A_t} = \frac{1}{M} \left\{ \frac{2 + (\gamma - 1)M^2}{(\gamma + 1)} \right\}^{\frac{\gamma + 1}{2(\gamma - 1)}}$$

Equation 1.4. Area Mach Relation

Accelerating the exhaust through the nozzle is limited by the pressure of the exhaust as it is accelerated. The pressure of the exhaust decreases as it is accelerated faster down the nozzle. If the pressure of the gas drops too low, the flow can separate off the surface of the nozzle, which restricts our expansion ratio.

$$\frac{P_c}{P} = \left(1 + \frac{\gamma - 1}{2} M^2 \right)^{\frac{\gamma}{\gamma - 1}}$$

Equation 1.5. Isentropic Pressure relations.

1.2 Obtaining Experimental Data

To understand how all these components combine to affect the performance of a rocket engine is a task that computational modeling has not quite reached. Rocket engines are an extremely complex system and have many different areas of losses due to combustion and real flow effects. Some of the real effects that could decrease performance of the rocket engine: Combustion inefficiencies, two phase flow, boundary layer growth, systems cooling, flow separation, under/overexpansion. Research to understand how even individual parameters can affect engine performance is often conducted using experimental results. [3,20] Experiments of full-scale motors is often relied on to test performance of motors and propellants. Conducting these tests to obtain data is expensive, timely, and potentially dangerous.

Some state-of-the-art models have been created to model the delivered specific impulse of rocket motors. The Solid Performance Program SPP models two phase flow, divergence, boundary layer, and chemical kinetic losses. [21,22] While models such as SPP attempt to understand the physics occurring within an engine at a high level, I look to apply data science tools and machine learning models to learn from experiments.

1.3 Applying Data Science Tools and Machine Learning

To apply data science tools and build machine learning models, I collected data from the open literature that reported delivered specific impulse, properties of the motor configuration, and the propellant being used. I used random forests to model how the propellant and the motor configuration effected the delivered specific impulse. To understand the ideal specific impulse, a similar dataset was used and PNNs were used to learn interpretable expressions.

Through collecting open literature data of delivered specific impulse, I find that the available data is extremely sparse, and few details are well reported. Data reported is often only high-performing propellants and the models learn to make accurate predictions without propellant information. To support this work, as much usable literature data was collected.

2. METHODS

2.1.1 Delivered Specific Impulse Data

For the delivered specific impulse database, 66 experimental motor tests were collected from the open literature. Literature sources needed to have information on both the propellant used and the motor configuration used in the test. The following information was required from each source: Propellant formulation and Ideal Specific Impulse, motor operating pressure, throat area, and motor dimensions. Some of the information, such as Ideal Specific Impulse, was calculated using NASA CEA [6] when this information was not provided by the publisher. Motor dimensions from datasets that used standard BATES motors [23–25] were required to be reported in the dataset. In total, 66 usable datasets were found within the open literature.

Table 2.1. Sample of open literature data collected for the delivered specific impulse models.

Motor #	% AP	% AN	% Al	Exit Angle (degrees)	Throat Diameter (in)	Expansion Ratio	Pressure (psia)	Ideal Specific Impulse	Delivered Specific Impulse
1	73	0.0	15.0	16.8	2.32	33.3	377.0	312.0	288.3
2	73	0.0	15.0	16.1	2.75	28.0	322.0	308.7	284.0
3	73	0.0	15.0	16.5	3.43	40.0	731.0	315.6	289.7
4	73	0.0	15.0	15.6	2.61	26.8	515.0	308.4	281.2
5	73	0.0	15.0	14.9	2.84	54.0	602.0	320.2	293.2
6	73	0.0	15.0	14.3	3.27	51.2	612.0	319.4	293.6

Some literature sources reported far more information than others and features were only considered if all literature sources reported the feature.

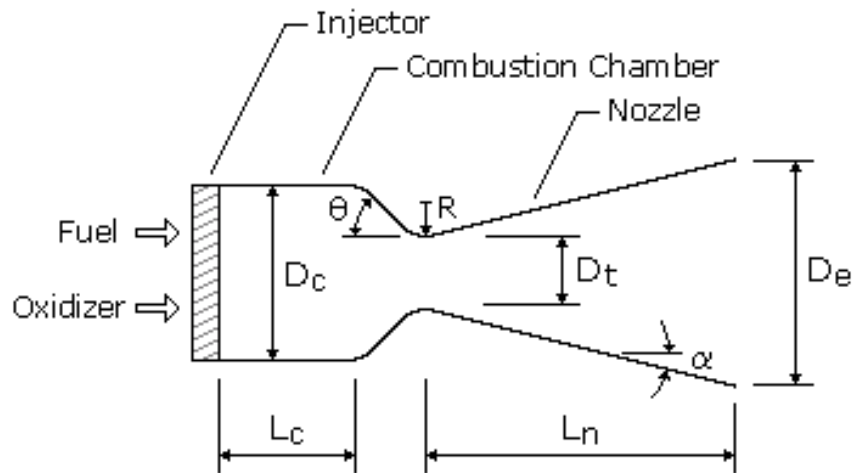


Figure 1.4

Figure 2.1. This figure depicts certain parts of a rocket engine and nozzle that are in the data columns. [26]

A cross section view of a rocket engine and nozzle can be seen in the image above. The properties that are used in the model are highlighted in the image. Many more properties are likely to be relevant in the predict of the delivered specific impulse but are rarely, if at all, reported in motor tests.

2.1.2 Ideal Specific Impulse Data

As mentioned above, Ideal specific impulse measures the theoretical max performance of a rocket motor. Ideal specific impulse is often calculated using thermochemical codes, such as NASA CEA and Cheetah and therefor can be collected from many sources. [27] Another study done recently looked to model the Ideal specific impulse of different propellants using regression models and the dataset from this study was used in the following work [16]. The a, b, c, and d variables represent the number of Carbon, Hydrogen, Nitrogen, and Oxygen atoms respectively.

Table 2.2. A sample of the data used for the ideal specific impulse models.

Chemical Formula	a	b	c	d	Heat of Formation	Moles Per Gram	Heat of Combustion	Specific Impulse (Ns/g)
C5H8N4O12	5.000	8.000	4.000	12.000	-128.70	0.0316	1.514	2.58
C7H5N3O6	7.000	5.000	3.000	6.000	-16.00	0.0253	1.291	2.11
C4H8N8O8	4.000	8.000	8.000	8.000	17.93	0.0338	1.477	2.62
C3H6N6O6	3.000	6.000	6.000	6.000	14.71	0.0338	1.482	2.62
C7H5N5O8	7.000	5.000	5.000	8.000	4.67	0.0270	1.420	2.35
CH3NO2	1.000	3.000	1.000	2.000	-27.00	0.0369	1.364	2.46

The Ideal specific impulse was determined at a chamber pressure and nozzle exit pressure of 68.9 and 1 bar [16].

2.2 Random Forest Models

Random Forest models are an ensemble of decision trees used to overcome the downsides of individual decision trees. [28] Individual decision trees are prone to overfitting but by using a large set of randomly generated trees, a random forest can overcome the faults of individual trees. For this work, I built random forests using the sklearn python package. [29]

Each tree is built from a random sample of the entire training set. Trees split the training data at each branch based upon a random selection of the features in the data. This process is repeated over and over until the data cannot be split anymore. Each individual tree makes its own prediction and the forest averages each of these predictions.

2.3 Parsimonious Neural Networks and Genetic Algorithms

Neural networks, NNs, are a machine learning method that use layers of nodes and functions to model complex and non-linear relationships. Many of the functions used in NNs, such as Relu, Sigmoid, Hyperbolic Tangent, etc., are rarely found in common chemistry or physics relations. This motivates us to create custom networks that can model common relations found in chemistry and physics. As mentioned, PNNs are constructed from custom neural networks that allow for a larger range of potential expressions than standard networks. [30] Unlike standard neural networks, each node can have a unique activation function and unique number of connections to the previous layer. This unique set of activation functions and connections allow the structure to build a wide range of different expressions. The output of a node is calculated using the following expression:

$$Y = f \left(\sum_{i=1}^N (X_i w_i) + b \right)$$

Equation 2.1. Activation function calculation.

Where Y is the output of a node, f is the activation function, N is the number of nodes in the previous layer, X_i are inputs from the previous layer, w_i are the weights multiplied to each input, and b is a bias term. The above expression works for many potential activation functions such as: Linear, Multiple, squared, etc. There are some activation functions where this expression will not work, such as the multiply activation function. For this activation function, the following expression must be used, where only inputs with non-zero weights and/or biases are included in the product.

$$Y = f \left(\left(\prod_{i=1}^{N-1} X_i * w_i \right) (w_N + b) \right)$$

Equation 2.2. Custom multiply activation function.

For any activations involving an even root, it is possible for many networks to fail during training due to a negative input being passed to an even root. To account for this, a constraint node is attached that uses a unique activation function and trains all even root activations to output real numbers only.

$$E(X_i) = ReLu \left(-sign \left(\sum_{i=1}^N X_i * w_i + b \right)^{even\#} \sqrt{\left| \sum_{i=1}^N X_i * w_i + b \right|} \right)$$

Equation 2.3. Even root activation function.

$$C = sum(E)$$

Equation 2.4. Constraint activation function.

Just like the activation function, the weights, and biases each have a list of potential values. The weights and biases can be set to a fixed value of zero, a fixed constant, or a randomly initialized value that is trained through backpropagation. Any number of constants (ie. 1, 2, π) can be added for weights and biases and any number of activation functions can be added. Increasing number of activations, weight/bias options, and network size increases the dimensions of the space of potential networks and thus the time for the genetic algorithm to optimize the network structure. Selecting meaningful activations and constant weight/bias options is extremely important to reduce this dimension to something reasonable. The components of each PNN are described using a list of integers that represent the different activation functions and weight/bias option. The PNN structure is then optimized using a genetic algorithm. The genetic algorithm uses an objective function that balance accuracy of the model with the complexity of the model.

$$Obj = f_1(E_{Test}) + p \left(\sum_{i=1}^{N_N} w_i + \sum_{j=1}^{N_w} w_j \right)$$

Equation 2.5. Objective function of genetic algorithm.

Here, E_{test} represents error of the trained PNN on the test set and f_1 represents a logarithmic function used in some cases to convert a wide range of errors to a similar order of magnitude to the terms representing the parsimony. The second term sums over the N_N neurons in the network and is intended to prefer simple activation functions. For example, if activation functions such as *linear, multiplication, $\sqrt{\quad}$, and $\sqrt[4]{\quad}$* are considered the corresponding scores can be $w_i = 0, 1, 2,$ and $3,$ respectively. The third term sums over all weights and biases (N_w) and is intended to prefer fixed, simple parameters over trainable ones. For example, parameters fixed to a value 0 are scored with a 0, non-zero fixed parameters are scored with a 1, and trainable parameters are scored with a 2. The models balance complexity and accuracy using the parsimony term, p . The larger the parsimony term is, the more the complexity of the model is valued and the smaller the parsimony term is, the more the model accuracy is valued. Using a range of parsimony values, we can discover a family of expressions with different levels of complexity and accuracy.

3. DELIVERED SPECIFIC IMPULSE

I constructed random forest models to predict the delivered specific impulse of a rocket motor configuration and propellant. These models can make predictions for aluminized composite solid rocket propellants only. The mean average error (MAE) was calculated using a 5-fold cross-validation. The MAE is calculated for each of the testing sets and averaged across the folds. The models each receive information on the composition of the propellant and some information on the motor configuration.

Table 3.1. Inputs for Models 1 and 2

Model 1	Model 2
Motor Operating Pressure	Motor Operating Pressure
Expansion Ratio	Expansion Ratio
Throat Diameter	Throat Diameter
Exit Angle	Exit Angle
Ideal Isp	%AP
	%AN
	%Al

Model 1 and 2 each receive different forms of the composition. Model 1 receives the Ideal specific impulse, which is either reported in the literature or calculated using CEA. [6] Model 2 receives the weight percentages of the major components of the propellant. The data the model see consists of propellants that are all made from these main ingredients.

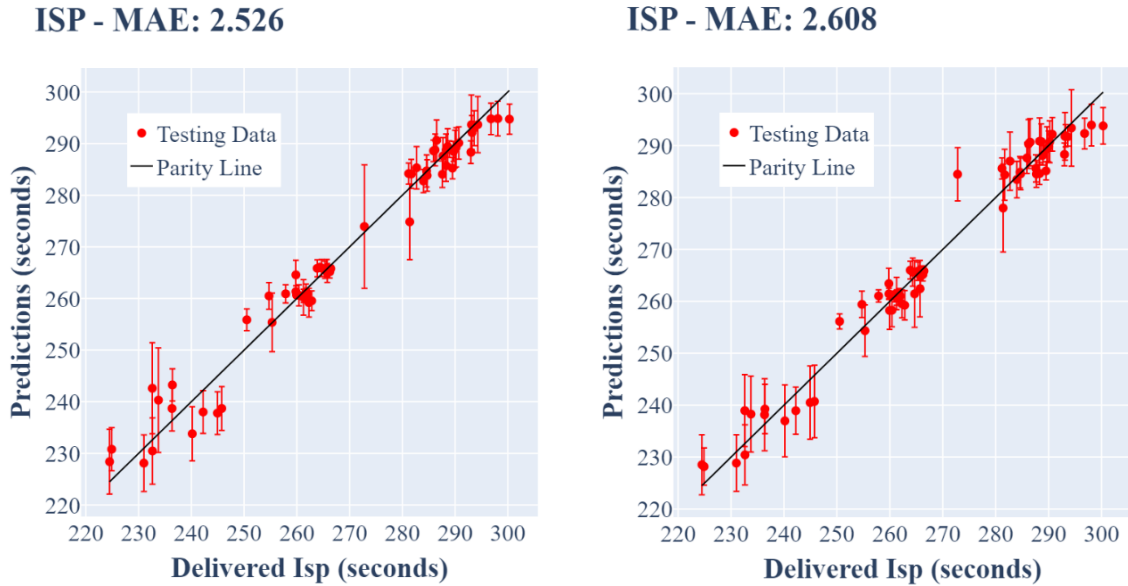


Figure 3.1. Parity plot for model 1 and 2.

The delivered specific impulse ranges from ~225-300 seconds in the available data. Models 1 and 2 perform very similarly with a MAE of less than 3 seconds. To confirm the performance of the models, I vary some of the input parameters over a range seen in the literature data. The variation in the input parameters shows the models knowledge of the input space and how the inputs affect the delivered specific impulse. To conduct the exercising of these models, the models are trained on all the data and a set of generated parameters is passed to the model for evaluation.

Table 3.2. Range of testing properties and some of the training data used.

Type	Nozzle Exit Angle	Throat Diameter (in)	Expansion Ratio	Pressure (psia)	Ideal Specific Impulse (sec)
Testing Range	15	2	9.5	1000	265-325
Exact Training Match (Green)	15	2	9.5	1000	~283-292
Similar Training Match (Red)	15	Varies	Varies	Varies	Varies

Model 1 is evaluated by varying the ideal specific impulse over a set motor configuration and motor operating pressure. The green training data represents datapoints that have the exact motor configuration and operating pressure as the testing range. Red represents data points with similar input parameters.

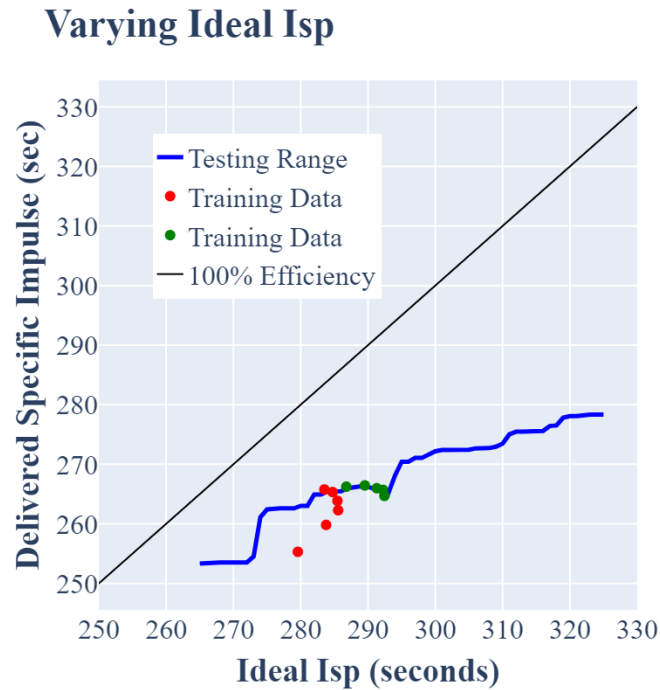


Figure 3.2. This figure depicts model 1s prediction of a range of ideal specific impulse.

Using a fixed sized motor configuration, I can observe how the model understands how variation in Ideal specific impulse changes the delivered specific impulse. The overlaid training points show us that the model is lacking training data in a large portion of the input space for this motor configuration and operating pressure. Although the model performs well on the training data, the random forest is extrapolating for much of the input space.

Table 3.3. Training data points values.

Motor Config.	Nozzle Exit Angle	Throat Diameter (in)	Expansion Ratio	Pressure (psia)	Color on Figure 3.3
Baseline	15	2	9.5	1000	Blue
1	15	2.164	9.24	1010	Red
2	15	2.119	9.39	946	Green
3	15	2.077	9.47	946	Yellow
4	15	1.904	9.59	964	Black
5	15	1.953	9.63	966	Gray
6	15	1.872	9.57	1136	Purple

The above table shows 6 different motor configurations and operating pressures that were seen in the training data. The percentage of ammonium perchlorate is varied from 60-75 percent. Model 2 is used to understand how the amount of ammonium perchlorate changed the delivered specific impulse. The amount of AN is adjusted a constant solid loading of 90, 0 percent aluminum, and the following equations.

$$\text{Solids Loading} = \%AP + \%Al + \%AN$$

Equation 3.1. Solids loading relationship.

Distribution of Testing Data

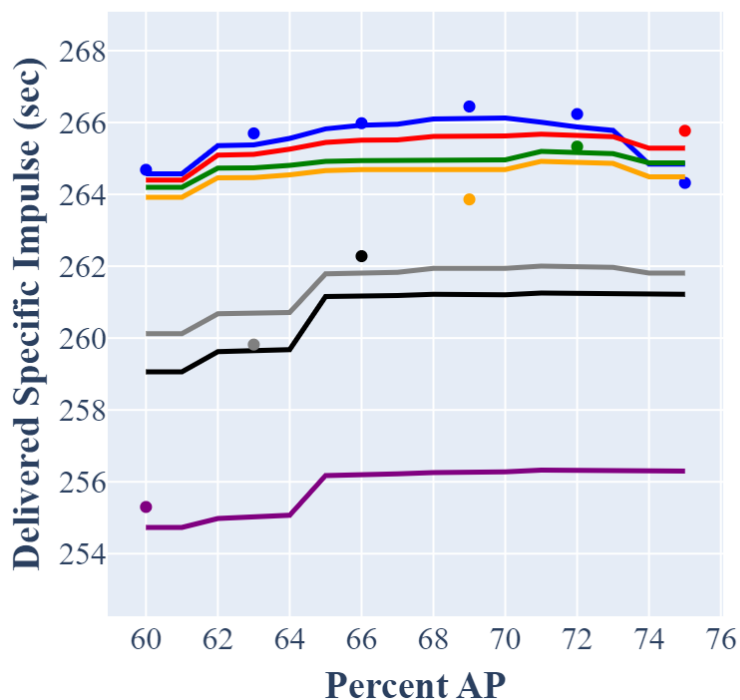


Figure 3.3. This figure depicts model 2's prediction for a range of AP and AN over a variety of motor configurations.

Using a variety of motor configurations, we can observe how the percentage of ammonium perchlorate and ammonium nitrate affect the delivered specific impulse. The colored lines and dots show which motor configuration and operation pressure is being evaluated. The dots represent the training points, and the lines represent the range of model evaluation. Again, we can observe that the training points cover far from enough of the input space for the model to avoid extrapolating. The model's accuracy in the areas of little to no testing data is uncertain.

The models perform well for a small amount of data and little variation within the propellant types. To verify the model and data quality, I remove some of the inputs to the models and observe their performance. The models should be unable to make accurate predictions if enough of the input's columns are removed.

Table 3.4. Model 3 and 4 inputs.

Model 3	Model 4
Motor Operating Pressure	Expansion Ratio
Expansion Ratio	Throat Diameter
Throat Diameter	Exit Angle
Exit Angle	

To create the inputs for models 3 and 4, I remove important inputs that were given to models 1 and 2. For model 3, all propellant composition information is removed. Ideal specific impulse is removed from model 1 and the weight percentages are removed from model 2. For model 4, the operating pressure is also removed, and it is interesting to note that model 4 only contains inputs of the motor configuration.

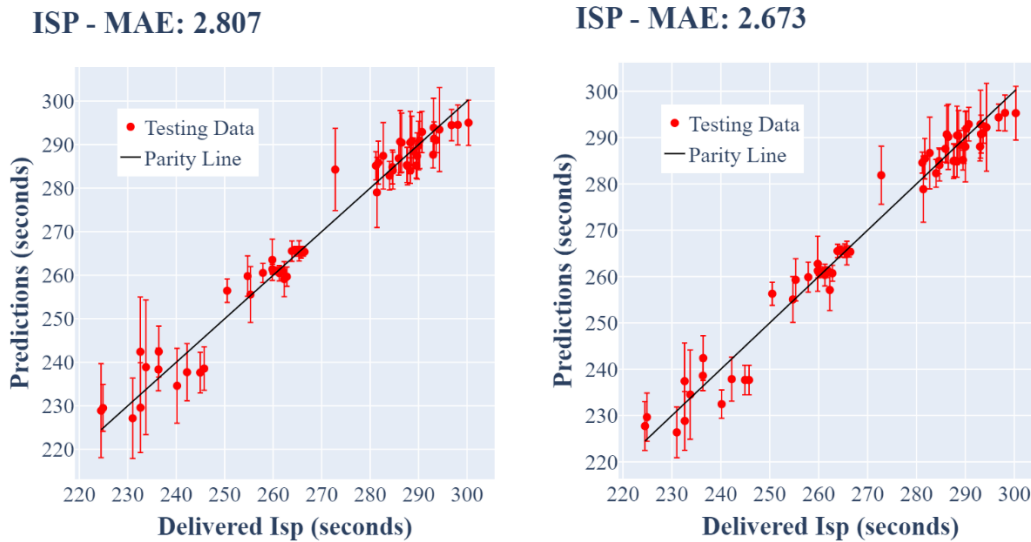


Figure 3.4. Parity plot for model 3 and model 4.

Model 3 makes accurate predictions of the data using no propellant information and only motor geometry and operating pressure. Model 4 also makes accurate prediction using on the geometry of the motor. The models with no information on what propellant is being used can predict almost as good as the models with propellant and motor information. This reveals that, in the available data, I can accurately predict what the delivered specific impulse is. This reveals that the data the models are evaluated on is heavily biased toward similar performing propellants.

4. IDEAL SPECIFIC IMPULSE

4.1 KJ Inputs

I constructed custom neural networks, PNNs, to find optimal expressions to calculate ideal specific impulse. These models can predict ideal specific impulse for any CHNO propellant. The operating pressure and the chamber pressure are fixed at a 68.9:1 ratio. A 5 k-fold cross-validation is used on the testing and training sets. The total RMSE is the averaged across the folds. The parsimony value is varied over a range that fills in an entire pareto front.

Using the inputs described by the Kamlet and Jacobs decomposition assumptions, I discovery a family of interpretable models. [15] The MLRA equation is displayed on the pareto front and is rediscovered in the evaluated equations. [16] The backpropagation of the network fails to optimize the weights and biases for the MLRA equation.

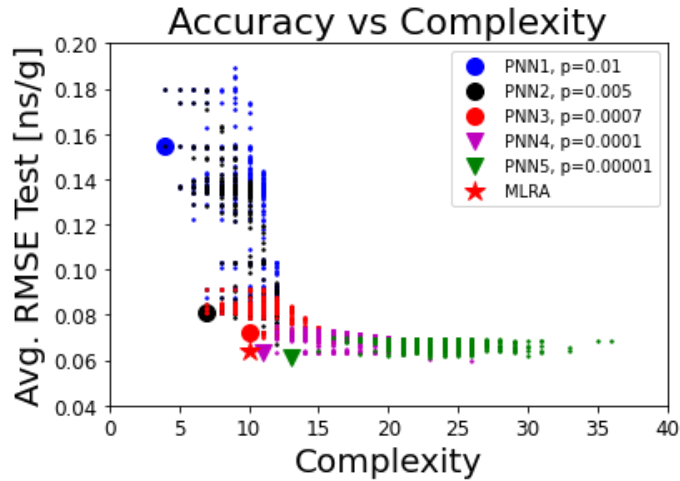


Figure 4.1. Pareto Front: KJ Inputs

$$PNN1 = w_1 N_g + Q$$

$$PNN2 = w_1 N_g + w_2 Q + b_1$$

$$PNN3 = \sqrt{b_1 + w_1 N_g + w_2 Q} = MLRA$$

$$PNN4 = \sqrt{w_1 M_g + w_2 N_g + w_3 Q}$$

$$PNN5 = \sqrt{w_1 M_g + w_2 N_g + w_3 Q + b_1}$$

In most machine learning models, inputs are normalized to avoid any large differences in the magnitudes of the different inputs. I use a min-max normalization technique to create KJ inputs with normalized values. In the pareto front, I again discover a family of interpretable models but do not rediscover the MRLA equation within this family.

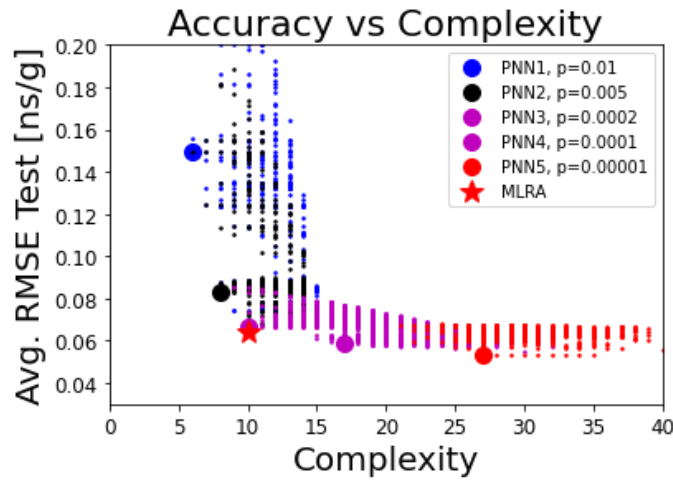


Figure 4.2. Pareto Front: KJ Inputs Normalized

$$PNN1 = w_1 Q + b_1$$

$$PNN2 = w_2 (w_1 N_g + Q) + b_1$$

$$PNN3 = w_2 (M + b_1) + w_3 (w_1 N_g + Q)$$

$$PNN4 = \sqrt{N + (w_1 M_g + w_2 N_g + Q + b_1)}$$

4.2 CHNO Inputs

In the above models, the Kamlet and Jacobs decomposition assumption is used to create inputs for the models. I now remove this assumption and break down the KJ inputs into the basic parameters used in their equations. These new inputs are the heat of formation and the number of

atoms for Carbon, Hydrogen, Nitrogen, and Oxygen. This new set of inputs still allows the PNN models to rediscover the MRLA equation and find other models that do not assume the same decomposition as the KJ inputs.

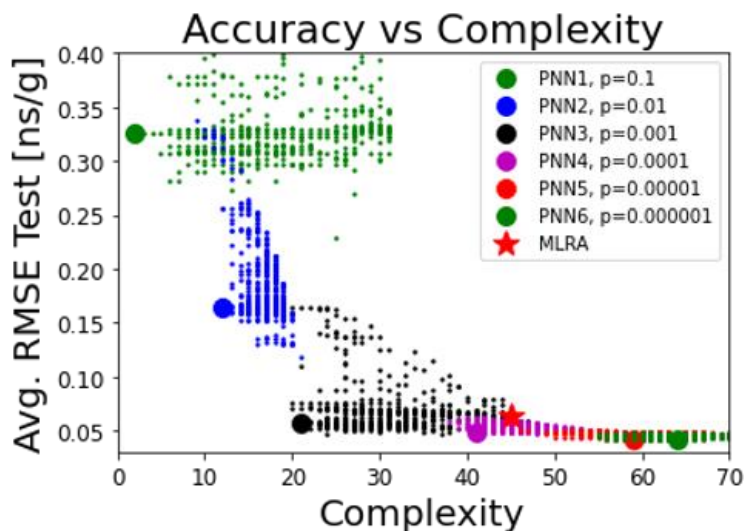


Figure 4.3. Pareto Front: CHNO Inputs

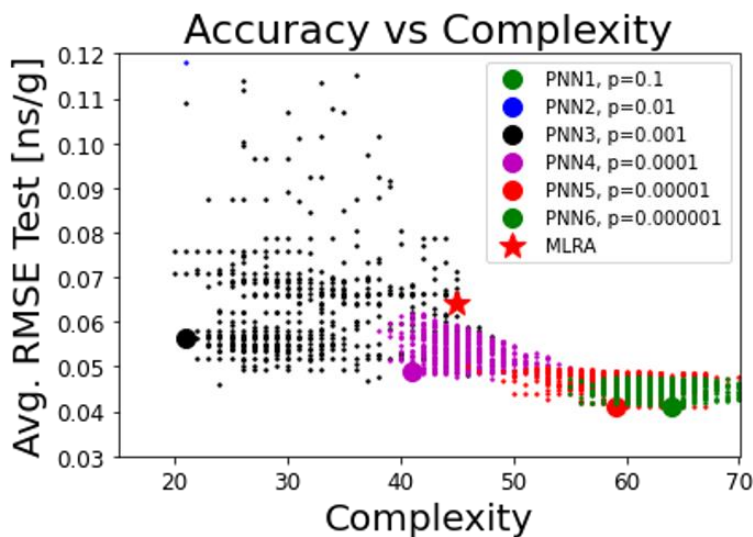


Figure 4.4. Pareto Front: CHNO Inputs zoomed in around MLRA

Using the CHNO inputs, I again discover a family of interpretable models to calculate ideal specific impulse. Removing the KJ decomposition assumption allows me to discover models that

perform better than the MLRA expression in both complexity and RMSE. The highest parsimony value discovers that the data can always be simple represented by the average of the data. A wide range of complex functions is discovered by the CHNO pareto front.

$$PNN3 = \sqrt{\frac{w_4H + b + c + w_3d}{w_1a + c + w_2d}}$$

PNN3, outperforms the MLRA equation in accuracy still using a slightly slower complexity. This model is particularly interesting because it follows a similar yet simpler structure of the MLRA equation.

5. CONCLUSION

5.1 Delivered Specific Impulse

The goal of this study was to create models that can accurately predict the delivered specific impulse of an aluminized solid rocket motor. The current trend of publication and sharing of data from tests is biased towards high performing propellants only. This has caused the rocket performance literature data that is currently available to not be sufficient to train intelligent ML models in the complex physical and thermochemical environment. For ML to be successful in this field, researchers need to publish all data, both good and bad, that accompany their studies.

5.2 Ideal Specific Impulse

The goal of this study was to evaluate the KJ assumption in the prediction of delivered specific impulse and investigate for expressions that do not use this assumption. A family of models is discovered that use the KJ decomposition assumptions and can make more accurate predictions than the state-of-the-art models. The MLRA equation performs well compared to other discovered equations that use the KJ decomposition assumption. Another family of models can be discovered that do not use the Kamlet and Jacobs decomposition assumptions. This family can make more accurate predictions than the models that rely on the KJ assumptions. In this family of models, we find many models that outperform the state-of-the-art models in both complexity and accuracy.

APPENDIX A. DELIVERED SPECIFIC IMPULSE DATA[2,25,31,32]

Motor No.	% A P	% A N	% Al	Nozzle Exit Angle	Throat Diameter (in)	Expansion Ratio	Pressure (psia)	Ideal Specific Impulse (sec)	Delivered Specific Impulse (sec)
1	73	0.0	15.0	16.8	2.32000	33.30	377.0	312.0000	288.30000
2	73	0.0	15.0	16.1	2.75000	28.00	322.0	308.7000	284.00000
3	73	0.0	15.0	16.5	3.43000	40.00	731.0	315.6000	289.70000
4	73	0.0	15.0	15.6	2.61000	26.80	515.0	308.4000	281.20000
5	73	0.0	15.0	14.9	2.84000	54.00	602.0	320.2000	293.20000
6	73	0.0	15.0	14.3	3.27000	51.20	612.0	319.4000	293.60000
7	73	0.0	15.0	16.7	9.63000	24.80	443.0	306.8000	287.60000
8	73	0.0	15.0	13.6	6.88000	23.60	507.0	306.0000	284.70000
9	73	0.0	15.0	17.0	6.88000	42.70	507.0	316.4000	293.00000
10	73	0.0	15.0	20.0	6.88000	87.90	523.0	327.0000	300.30000
11	68	0.0	16.4	20.0	2.41000	47.30	683.0	315.8000	286.20000
12	68	0.0	16.4	19.9	2.12000	55.60	670.0	318.2000	286.50000
13	68	0.0	16.4	19.7	2.10000	96.90	733.0	325.8000	293.10000
14	68	0.0	18.0	14.7	7.09000	33.10	549.0	312.3000	287.70000
15	70	0.0	16.0	14.1	3.36000	51.20	568.0	317.1000	290.70000
16	70	0.0	16.0	13.6	4.36000	29.80	545.0	308.5000	284.60000
17	72	0.0	16.0	14.0	4.24000	32.10	547.0	311.1000	289.50000
18	70	0.0	16.0	12.8	3.82000	39.30	588.0	313.0000	288.90000
19	69	0.0	16.0	20.0	2.99000	17.50	642.0	294.9000	272.80000

20	70	0.0	16. 0	14.2	1.44000	55.00	788.0	318.300 0	290.00000 0
21	70	0.0	16. 0	13.9	1.93000	50.70	645.0	317.000 0	288.60000 0
22	70	0.0	16. 0	14.1	2.50000	35.40	485.0	311.300 0	285.90000 0
23	72	0.0	16. 0	14.8	2.82000	46.00	465.0	317.100 0	290.20000 0
24	70	0.0	16. 0	20.0	2.41000	47.00	676.0	315.900 0	288.30000 0
25	71	0.0	18. 0	14.6	3.57000	64.60	609.0	324.800 0	296.80000 0
26	59	0.0	20. 0	14.6	3.32000	74.70	723.0	329.700 0	298.10000 0
27	69	0.0	16. 0	15.0	1.35000	40.20	367.0	309.700 0	282.70000 0
28	69	0.0	16. 0	15.0	1.36000	149.30	356.0	325.700 0	294.30000 0
29	7	0.0	19. 0	18.0	3.16000	25.10	454.0	304.900 0	281.70000 0
30	7	0.0	19. 0	15.0	6.67000	17.90	344.0	297.500 0	281.40000 0
A-4	75	0.0	15. 0	15.0	2.16400	9.24	1010.0	283.510 0	265.77000 0
A-5	72	0.0	18. 0	15.0	2.11900	9.39	946.0	284.740 0	265.33000 0
A-6	69	0.0	21. 0	15.0	2.07700	9.47	946.0	285.450 0	263.86000 0
A-7	66	0.0	24. 0	15.0	1.90400	9.59	964.0	285.560 0	262.28000 0
A-8	63	0.0	27. 0	15.0	1.95300	9.63	966.0	283.770 0	259.82000 0
A-9	60	0.0	30. 0	15.0	1.87200	9.57	1136.0	279.570 0	255.30000 0
B-4	75	0.0	15. 0	15.0	1.24100	9.22	1022.0	283.480 0	262.81000 0
B-5	72	0.0	18. 0	15.0	1.21500	9.36	943.0	284.650 0	261.27000 0
B-6	69	0.0	21. 0	15.0	1.19100	9.42	934.0	285.300 0	259.83000 0
B-7	66	0.0	24. 0	15.0	1.09400	9.53	1001.0	285.450 0	257.88000 0
B-8	63	0.0	27. 0	15.0	1.12100	9.57	973.0	283.630 0	254.73000 0
B-9	60	0.0	30. 0	15.0	1.07000	9.56	1117.0	279.450 0	250.51000 0

F1P15	75	0.0	15.0	15.0	1.00000	9.50	1000.0	283.0581	261.262626
F2P15	72	0.0	18.0	15.0	1.00000	9.50	1000.0	286.7686	261.733701
F3P15	69	0.0	21.0	15.0	1.00000	9.50	1000.0	289.5209	261.958510
F4P15	66	0.0	24.0	15.0	1.00000	9.50	1000.0	291.2946	260.970832
F5P15	63	0.0	27.0	15.0	1.00000	9.50	1000.0	292.2324	260.408292
F6P15	60	0.0	30.0	15.0	1.00000	9.50	1000.0	292.4363	259.946627
F1P70	75	0.0	15.0	15.0	2.00000	9.50	1000.0	283.0581	264.319654
F2P70	72	0.0	18.0	15.0	2.00000	9.50	1000.0	286.7686	266.235968

APPENDIX B. IDEAL SPECIFIC IMPULSE DATA[16]

Chemical Name	Chemical Formula	a	b	c	d	Heat of Formation	Moles Per Gram	Heat of Combustion	Specific Impulse (Ns/g)
PETN	C ₅ H ₈ N ₄ O ₁₂	5.000	8.000	4.000	12.000	-128.70	0.0316	1.514	2.58
TNT	C ₇ H ₅ N ₃ O ₆	7.000	5.000	3.000	6.000	-16.00	0.0253	1.291	2.11
HMX	C ₄ H ₈ N ₈ O ₈	4.000	8.000	8.000	8.000	17.93	0.0338	1.477	2.62
RDX	C ₃ H ₆ N ₆ O ₆	3.000	6.000	6.000	6.000	14.71	0.0338	1.482	2.62
Tetryl	C ₇ H ₅ N ₅ O ₈	7.000	5.000	5.000	8.000	4.67	0.0270	1.420	2.35
NM	CH ₃ NO ₂	1.000	3.000	1.000	2.000	-27.00	0.0369	1.364	2.46
HNS	C ₁₄ H ₆ N ₆ O ₁₂	14.000	6.000	6.000	12.000	18.70	0.0233	1.367	2.19
Comp-B	C _{2.03} H _{2.64} N _{2.18} O _{2.67}	2.030	2.640	2.180	2.670	1.28	0.0308	1.410	2.42
PBX-9011	C _{1.73} H _{3.18} N _{2.45} O _{2.61}	1.730	3.180	2.450	2.610	-4.05	0.0333	1.358	2.43
LX-14	C _{1.52} H _{2.92} N _{2.59} O _{2.66}	1.520	2.920	2.590	2.660	1.50	0.0336	1.423	2.54
Pentolite(50/50)	C _{2.33} H _{2.37} N _{1.29} O _{3.22}	2.330	2.370	1.290	3.220	-23.90	0.0285	1.402	2.37
HNAB	C ₁₂ H ₄ N ₈ O ₁₂	12.000	4.000	8.000	12.000	67.90	0.0243	1.445	2.32
NG	C ₃ H ₅ N ₃ O ₉	3.000	5.000	3.000	9.000	-88.60	0.0319	1.591	2.53
NQ	CH ₄ N ₄ O ₂	1.000	4.000	4.000	2.000	-22.10	0.0385	0.898	2.11
Octol (75/25)	C _{1.78} H _{2.58} N _{2.36} O _{2.69}	1.780	2.580	2.360	2.690	2.78	0.0317	1.431	2.50
TATB	C ₆ H ₆ N ₆ O ₆	6.000	6.000	6.000	6.000	-36.85	0.0291	1.075	2.01
PA	C ₆ H ₃ N ₃ O ₇	6.000	3.000	3.000	7.000	-51.30	0.0251	1.283	2.18

Cyclotol	C2.04H2.50N2.1 5O2.68	2.0 40	2.5 00	2.1 50	2.6 80	1.15	0.0 304	1.406	2.42
DEGDN	C4H8N2O7	4.0 00	8.0 00	2.0 00	7.0 00	-99.40	0.0 332	1.392	2.42
PBX-9007	C1.97H3.22N2.4 3O2.44	1.9 70	3.2 20	2.4 30	2.4 40	7.13	0.0 324	1.392	2.39
PBX-9501	C1.47H2.86N2.6 0O2.69	1.4 70	2.8 60	2.6 00	2.6 90	2.28	0.0 336	1.442	2.56
DIPAM	C12H6N8O12	12. 000	6.0 00	8.0 00	12. 000	-6.80	0.0 253	1.298	2.16
BTNEU	C5H6N8O13	5.0 00	6.0 00	8.0 00	13. 000	-76.91	0.0 311	1.467	2.52
BTTN	C4H7N3O9	4.0 00	7.0 00	3.0 00	9.0 00	-97.04	0.0 322	1.509	2.59
FOX-7	C2H4N4O4	2.0 00	4.0 00	4.0 00	4.0 00	-32.00	0.0 338	1.199	2.38
DDNP	C6H2N4O5	6.0 00	2.0 00	4.0 00	5.0 00	46.39	0.0 238	1.391	2.27
DNDMOxm	C4H6N4O6	4.0 00	6.0 00	4.0 00	6.0 00	-73.00	0.0 316	1.171	2.22
DNOC	C7H6N2O5	7.0 00	6.0 00	2.0 00	5.0 00	-47.80	0.0 253	1.109	1.93
DNPH	C6H6N4O4	6.0 00	6.0 00	4.0 00	4.0 00	11.95	0.0 278	1.173	2.07
DINA	C4H8N4O8	4.0 00	8.0 00	4.0 00	8.0 00	-65.88	0.0 333	1.472	2.56
DIPEHN	C10H16N6O19	10. 000	16. 000	6.0 00	19. 000	- 233.7 9	0.0 315	1.422	2.49
ETN	C6H11N3O9	6.0 00	11. 000	3.0 00	9.0 00	- 114.7 6	0.0 325	1.365	2.34
EDDN	C2H10N4O6	2.0 00	10. 000	4.0 00	6.0 00	- 156.1 8	0.0 403	0.966	2.20
EDNA	C2H6N4O4	2.0 00	6.0 00	4.0 00	4.0 00	-24.81	0.0 367	1.303	2.46
GUNI	CH6N4O3	1.0 00	6.0 00	4.0 00	3.0 00	-92.52	0.0 410	0.662	1.90
FOX-12	C2H7N7O5	2.0 00	7.0 00	7.0 00	5.0 00	-85.09	0.0 371	0.898	2.15
1a	C12H5N7O12	12. 000	5.0 00	7.0 00	12. 000	9.88	0.0 245	1.368	2.22
1b	C6H8N6O18	6.0 00	8.0 00	6.0 00	18. 000	- 161.5 3	0.0 310	1.609	2.48

1c	CH6N2O3	1.0 00	6.0 00	2.0 00	3.0 00	-84.31	0.0 426	0.947	2.16
1d	C6N6O6	6.0 00	0.0 00	6.0 00	6.0 00	144.5 0	0.0 238	1.692	2.65
1e	C2N8O4	2.0 00	0.0 00	8.0 00	4.0 00	207.5 3	0.0 300	1.978	2.90
1f	C2N6O3	2.0 00	0.0 00	6.0 00	3.0 00	161.0 2	0.0 288	1.936	2.95
1g	C2H8N10O4	2.0 00	8.0 00	10. 000	4.0 00	106.7 4	0.0 381	1.432	2.65
1h	CH4N6O3	1.0 00	4.0 00	6.0 00	3.0 00	36.33	0.0 372	1.344	2.61
1i	CHN5O3	1.0 00	1.0 00	5.0 00	3.0 00	73.76	0.0 324	1.681	2.65
1j	CH4N6O4	1.0 00	4.0 00	6.0 00	4.0 00	52.27	0.0 366	1.597	2.73
1k	C2H6N8O3	2.0 00	6.0 00	8.0 00	3.0 00	32.67	0.0 368	1.085	2.27
1l	C2H7N9O3	2.0 00	7.0 00	9.0 00	3.0 00	61.28	0.0 378	1.171	2.37
1m	C2H9N11O3	2.0 00	9.0 00	11. 000	3.0 00	112.6 9	0.0 394	1.286	2.49
1n	C2H4N6O2	2.0 00	4.0 00	6.0 00	2.0 00	56.96	0.0 347	1.198	2.30
1o	C2H7N7O3	2.0 00	7.0 00	7.0 00	3.0 00	67.38	0.0 381	1.391	2.54
1p	C5H3N5O10	5.0 00	3.0 00	5.0 00	10. 000	58.66	0.0 282	1.860	2.72
1q	CN2O2	1.0 00	0.0 00	2.0 00	2.0 00	43.90	0.0 278	1.915	2.74
1r	N6	0.0 00	0.0 00	6.0 00	0.0 00	345.6 0	0.0 357	4.114	4.22
1s	N8	0.0 00	0.0 00	8.0 00	0.0 00	406.7 0	0.0 357	3.631	4.11
1t	N10	0.0 00	0.0 00	10. 000	0.0 00	473.4 0	0.0 357	3.381	4.04
M1	C2.535H3.102N 0.894O3.370	2.5 35	3.1 02	0.8 94	3.3 70	-53.80	0.0 291	1.213	2.12
M1A1	C2.577 H3.237N0.862O 3.357	2.5 77	3.2 37	0.8 62	3.3 57	-57.40	0.0 292	1.179	2.07
M6	C2.467H3.015N 0.911O3.412	2.4 67	3.0 15	0.9 11	3.4 12	-53.80	0.0 292	1.228	2.16
M10	C2.214H2.854N 0.916O3.606	2.2 14	2.8 54	0.9 16	3.6 06	-59.30	0.0 298	1.256	2.27

M12	C2.309H2.922N 0.927O3.522	2.3 09	2.9 22	0.9 27	3.5 22	-56.80	0.0 296	1.245	2.23
M14	C2.406H2.940N 0.918O3.456	2.4 06	2.9 40	0.9 18	3.4 56	-54.10	0.0 292	1.242	2.20
IMR	C2.301H2.912N 0.927O3.527	2.3 01	2.9 12	0.9 27	3.5 27	-56.80	0.0 296	1.247	2.24
M2	C2.049H2.837N 0.986O3.669	2.0 49	2.8 37	0.9 86	3.6 69	-55.90	0.0 304	1.319	2.37
M5	C2.085H2.855N 0.970O3.655	2.0 85	2.8 55	0.9 70	3.6 55	-56.80	0.0 303	1.304	2.35
M7	C1.965H2.565N 1.065O3.683	1.9 65	2.5 65	1.0 65	3.6 83	-48.30	0.0 302	1.387	2.45
M8	C1.911H2.609N 1.075O3.710	1.9 11	2.6 09	1.0 75	3.7 10	-47.50	0.0 305	1.410	2.48
M9	C1.844H2.527N 1.091O3.751	1.8 44	2.5 27	1.0 91	3.7 51	-47.70	0.0 305	1.422	2.50
M18	C2.440H3.145N 0.885O3.446	2.4 40	3.1 45	0.8 85	3.4 46	-55.70	0.0 295	1.232	2.17
M26	C2.224H2.951N 1.006O3.515	2.2 24	2.9 51	1.0 06	3.5 15	-50.40	0.0 300	1.307	2.31
T25	C2.223H2.890N 0.989O3.532	2.2 23	2.8 90	0.9 89	3.5 32	-52.10	0.0 299	1.295	2.30
M15	C1.597H3.532N 2.586O2.565	1.5 97	3.5 32	2.5 86	2.5 65	-30.20	0.0 346	1.094	2.19
M17	C1.395H3.301N 2.602O2.718	1.3 95	3.3 01	2.6 02	2.7 18	-31.90	0.0 349	1.137	2.30
T35	C1.572H3.524N 2.552O2.614	1.5 72	3.5 24	2.5 52	2.6 14	-33.10	0.0 347	1.088	2.20
28/22.5/1.5/48 NC (12% N)/NG/Carbamite /Picrite	C1.490H3.273N 2.393O2.830	1.4 90	3.2 73	2.3 93	2.8 30	-37.56	0.0 343	1.131	2.28
28/22.5/1.5/48 NC (13.35% N)/NG/Carbamite /Picrite	C1.445H3.171N 2.420O2.846	1.4 45	3.1 71	2.4 20	2.8 46	-35.20	0.0 343	1.157	2.32
20.8/20.6/3.6/55 NC (13.35% N)/NG/Carbamite /Pi...	C1.468H3.369N 2.611O2.649	1.4 68	3.3 69	2.6 11	2.6 49	-32.00	0.0 347	1.107	2.25
28/22.5/1.5/38/10 NC (12% N)/NG/Carbamite \nPi...	C1.529H3.159N 2.278O2.908	1.5 29	3.1 59	2.2 78	2.9 08	-34.77	0.0 339	1.189	2.33
28/22.5/1.5/33/15 NC (12%	C1.548H3.102N 2.221O2.947	1.5 48	3.1 02	2.2 21	2.9 47	-33.38	0.0 336	1.219	2.36

N)/NG/Carbamite ^nPi...										
28/22.5/1.5/28/20 NC (12% N)/NG/Carbamite ^nPi...	C1.568H3.045N 2.164O2.986	1.5 68	3.0 45	2.1 64	2.9 86	-31.98	0.0 334	1.248	2.38	
29.5/32/8/1/29.5 DNC/NG/DEP/2- NDPA/RDX	C1.996H2.942N 1.490O3.261	1.9 96	2.9 42	1.4 90	3.2 61	-35.30	0.0 311	1.339	2.38	
29.5/32/2/1/29.5/ 6 DNC/NG/DEP/2- NDPA/RDX^nB DN...	C1.813H2.808N 1.565O3.341	1.8 13	2.8 08	1.5 65	3.3 41	-33.23	0.0 316	1.390	2.47	
29.5/32/8/1/29.5 DNC/NG/DEP/2- NDPA/ADN	C1.598H3.096N 1.644O3.416	1.5 98	3.0 96	1.6 44	3.4 16	-45.82	0.0 331	1.314	2.45	
29.5/32/8/1/29.5 DNC/NG/DEP/2- NDPA/HNF	C1.759H2.951N 1.499O3.431	1.7 59	2.9 51	1.4 99	3.4 31	-40.03	0.0 320	1.372	2.47	
30/40/30 DNC/CL/TAGA Z	C1.908H3.576N 2.448O2.448	1.9 08	3.5 76	2.4 48	2.4 48	-16.68	0.0 334	1.177	2.18	
80/20 RDX/GAP	C1.687H3.171N 2.767O2.363	1.6 87	3.1 71	2.7 67	2.3 63	10.96	0.0 336	1.392	2.46	
71/9/20 RDX/GAP/BTT N	C1.564H2.953N 2.440O2.755	1.5 64	2.9 53	2.4 40	2.7 55	-0.96	0.0 334	1.445	2.55	
70/30 HMX/GAP	C1.854H3.406N 2.800O2.194	1.8 54	3.4 06	2.8 00	2.1 94	12.73	0.0 335	1.342	2.35	
80/20 RDX/BAMO	C1.600H2.940N 2.940O2.291	1.6 00	2.9 40	2.9 40	2.2 91	17.26	0.0 335	1.408	2.49	
70/30 HMX/BAMO	C1.725H3.059N 3.059O2.085	1.7 25	3.0 59	3.0 59	2.0 85	22.17	0.0 334	1.367	2.41	
70/30 CL- 20/GAP	C1.868H2.474N 2.826O2.220	1.8 68	2.4 74	2.8 26	2.2 20	23.89	0.0 314	1.416	2.44	
80/20 CL- 20/BAMO	C1.615H1.875N 2.970O2.321	1.6 15	1.8 75	2.9 70	2.3 21	29.56	0.0 312	1.488	2.58	
80/20 ADN/GAP	C0.606H3.589N 3.185O2.781	0.6 06	3.5 89	3.1 85	2.7 81	-17.55	0.0 388	1.326	2.60	
75/25 ADN/GAP	C0.758H3.681N 3.176O2.671	0.7 58	3.6 81	3.1 76	2.6 71	-14.69	0.0 384	1.307	2.57	
70/30 ADN/GA	C0.909H3.772N 3.166O2.560	0.9 09	3.7 72	3.1 66	2.5 60	-11.82	0.0 381	1.289	2.53	
65/35 ADN/GA	C1.061H3.863N 3.156O2.449	1.0 61	3.8 63	3.1 56	2.4 49	-8.96	0.0 377	1.270	2.48	

60/40 ADN/GAP	C1.212H3.955N 3.147O2.339	1.2 12	3.9 55	3.1 47	2.3 39	-6.09	0.0 373	1.252	2.42
50/50 ADN/GAP	C1.515H4.137N 3.127O2.117	1.5 15	4.1 37	3.1 27	2.1 17	-0.36	0.0 366	1.215	2.29
74/26 ADN/AB	C0.494H3.282N 2.880O3.153	0.4 94	3.2 82	2.8 80	3.1 53	-26.17	0.0 384	1.397	2.47
85/15 ADN/PMVT	C0.545H3.559N 3.286O2.741	0.5 45	3.5 59	3.2 86	2.7 41	-20.16	0.0 390	1.279	2.57
80/20 ADN/PVMDO	C0.588H3.756N 2.972O2.972	0.5 88	3.7 56	2.9 72	2.9 72	-23.21	0.0 391	1.367	2.62
75/25 AN/AB	C0.475H4.610N 2.349O3.548	0.4 75	4.6 10	2.3 49	3.5 48	-86.28	0.0 410	1.054	2.29
75/25 AN/PMVT	C0.545H5.066N 2.669O3.186	0.5 45	5.0 66	2.6 69	3.1 86	-88.16	0.0 420	0.889	2.24
85/15 AN/PVMDO	C0.441H5.130N 2.418O3.480	0.4 41	5.1 30	2.4 18	3.4 80	-92.66	0.0 423	0.986	2.34
60/20/20 AN/GAP/TMET N	C0.998H4.714N 2.340O3.156	0.9 98	4.7 14	2.3 40	3.1 56	-112.4 1	0.0 393	0.614	1.85
70/15/15 AN/GAP/TMET N	C0.749H4.785N 2.380O3.304	0.7 49	4.7 85	2.3 80	3.3 04	-111.5 6	0.0 404	0.696	2.01
60/15/15/10 AN/GAP/TMET N/NC(12%N)	C0.976H4.578N 2.216O3.290	0.9 76	4.5 78	2.2 16	3.2 90	-107.2 4	0.0 390	0.721	1.99
40/15/15/30 AN/GAP/TMET N/NC(12%N)	C1.431H4.165N 1.887O3.262	1.4 31	4.1 65	1.8 87	3.2 62	-98.61	0.0 362	0.772	1.94
40/15/15/30 AN/GAP/TMET N/HMX	C1.154H4.096N 2.441O2.990	1.1 54	4.0 96	2.4 41	2.9 90	-77.04	0.0 374	0.856	2.08
80/20 HNF/GAP	C1.043H3.195N 2.791O2.824	1.0 43	3.1 95	2.7 91	2.8 24	-1.86	0.0 361	1.481	2.66
80/20 HNF/PGN	C0.941H3.025N 2.353O3.29	0.9 41	3.0 25	2.3 53	3.2 90	-18.95	0.0 358	1.522	2.65
80/20 HNF/PLN	C0.925H3.648N 2.347O3.272	0.9 25	3.6 48	2.3 47	3.2 72	-19.55	0.0 372	1.539	2.70
80/20 HNF/BAMO	C0.956H2.964N 2.964O2.752	0.9 56	2.9 64	2.9 64	2.7 52	4.44	0.0 360	1.498	2.68
80/20 HNF/HTPB	C1.852H4.315N 2.197O2.666	1.8 52	4.3 15	2.1 97	2.6 66	-10.29	0.0 351	1.383	2.40
85/15 1f/AB	C1.374H0.520N 3.557O2.074	1.3 74	0.5 20	3.5 57	2.0 74	85.02	0.0 295	1.853	2.88
85/15 3u/AB	C1.374H0.520N 3.557O2.074	1.3 74	0.5 20	3.5 57	2.0 74	60.58	0.0 295	1.609	2.72

85/15 3v/AB	C1.374H0.520N 3.557O2.074	1.3 74	0.5 20	3.5 57	2.0 74	76.92	0.0 295	1.772	2.83
85/15 1e/AB	C1.134H0.520N 3.687O2.140	1.1 34	0.5 20	3.6 87	2.1 40	85.49	0.0 304	1.889	2.86
69.7/0.6/14.79/14 .91 HAN/AN/MeOH /H2 O	C0.462H6.435N 1.466O4.215	0.4 62	6.4 35	1.4 66	4.2 15	- 141.3 4	0.0 445	0.915	2.27
77.25/0.67/17.19/ 4.89 HAN/AN/MeOH /H2 O	C0.537H5.940N 1.625O4.051	0.5 37	5.9 40	1.6 25	4.0 51	- 113.9 4	0.0 433	1.085	2.43
72.3/0.62/11.62/1 5.47 HAN/AN/EtOH/ H2 O	C0.505H6.274N 1.521O4.146	0.5 05	6.2 74	1.5 21	4.1 45	- 135.9 8	0.0 440	0.927	2.31
73.41/0.63/10.26/ 15.70 HAN/AN/ 1-PrOH/H2 O	C0.512H6.198N 1.544O4.124	0.5 12	6.1 98	1.5 44	4.1 24	- 133.4 9	0.0 439	0.938	2.31
63.63/0.54/22.22/ 13.61 HAN/AN/Glycin e/H2 O	C0.592H5.669N 1.635O4.018	0.5 92	5.6 69	1.6 35	4.0 18	- 142.3 3	0.0 425	0.771	2.15
60/30/10 ADN/MAN/Urea	C0.485H4.514N 2.905O3.058	0.4 85	4.5 14	2.9 05	3.0 58	-57.54	0.0 411	1.105	2.45
40/40/20 ADN/MAN/Urea	C0.758H5.172N 2.806O2.898	0.7 58	5.1 72	2.8 06	2.8 98	-73.95	0.0 415	0.902	2.20
30/40/30 ADN/MAN/Urea	C0.925H5.516N 2.817O2.742	0.9 25	5.5 16	2.8 17	2.7 42	-84.31	0.0 416	0.744	1.97
59.86/25/15.14 H2 O2 (70%)/AN/EtOH	C0.657H7.680N 0.625O4.727	0.6 57	7.6 80	0.6 25	4.7 27	- 172.8 5	0.0 460	0.908	2.27
80/8/12 H2 O2 (70%)/H2 O/EtOH	C0.521H8.410O 5.330	0.5 21	8.4 10	0.0 00	5.3 30	- 213.1 3	0.0 477	0.828	2.19
36.67/51.20/12.1 3 H2 O2 (70%)/ADN/EtO H	C0.527H5.962N 1.651O4.034	0.5 27	5.9 62	1.6 50	4.0 34	- 108.1 3	0.0 434	1.137	2.47
N2 O4 /HEH (O/F = 1.94)	C0.895H3.579N 2.330O3.317	0.8 95	3.5 79	2.3 30	3.3 17	-24.10	0.0 372	1.511	2.68
N2 O4 - UDMH/HEH (80/20) (O/F = 2.45)	C0.927H3.713N 2.471O3.161	0.9 27	3.7 13	2.4 71	3.1 61	-2.58	0.0 374	1.660	2.79

N2 O4 - UDMH/HEH (90/10) (O/F = 2.55)	C0.922H3.695N 2.482O3.156	0.9 22	3.6 95	2.4 82	3.1 56	-0.42	0.0 374	1.679	2.80
N2 O4 /UDMH (O/F = 2.60)	C0.927H3.707N 2.496O3.139	0.9 27	3.7 07	2.4 96	3.1 39	2.05	0.0 374	1.696	2.81
N2 O4 - UDMH/HEH (60/40) (O/F= 2.32)	C0.920H3.679N 2.439O3.196	0.9 20	3.6 79	2.4 39	3.1 96	-5.94	0.0 374	1.641	2.77
RFNA/UDMH (O/F = 2.92)	C0.850H4.559N 2.070O3.516	0.8 50	4.5 59	2.0 70	3.5 16	-43.83	0.0 393	1.460	2.68
RFNA- UDMH/HEH (90/10) (O/F = 2.85)	C0.850H4.557N 2.061O3.523	0.8 50	4.5 57	2.0 61	3.5 23	-45.77	0.0 393	1.444	2.67
RFNA/HEH (O/F = 2.14)	C0.837H4.408N 1.954O3.637	0.8 37	4.4 08	1.9 54	3.6 37	-64.32	0.0 390	1.304	2.57
O2 /RP-1 (O/F = 2.60)	C1.989H3.878O 4.513	1.9 89	3.8 78	0.0 00	4.5 13	-18.41	0.0 323	2.146	2.94
O2 /N2 H4 (O/F = 0.91)	H6.529N3.265O 2.981	0.0 00	6.5 29	3.2 65	2.9 81	15.16	0.0 476	1.905	3.07
O2 /Toluene (O/F = 1.87)	C2.644H3.021O 4.075	2.6 44	3.0 21	0.0 00	4.0 75	-5.19	0.0 279	2.026	2.84
O2 /Methylcyclohexa ne (O/F= 2.04)	C2.345H4.691O 4.194	2.3 45	4.6 91	0.0 00	4.1 94	-21.69	0.0 327	2.007	2.87
O2 /n-heptane (O/F = 2.05)	C2.291H5.238O 4.200	2.2 91	5.2 38	0.0 00	4.2 00	-24.03	0.0 341	2.017	2.88
O2 /Ethylene oxide (O/F = 1.10)	C2.157H4.313O 4.360	2.1 57	4.3 13	0.0 00	4.3 60	-29.72	0.0 326	1.985	2.87
O2 /Nitroethane (O/ F= 0.65)	C1.615H4.037N 0.807O4.077	1.6 15	4.0 37	0.8 07	4.0 77	-31.58	0.0 345	1.818	2.81
O2 /EtOH-75% (O/F = 1.30)	C1.413H5.445O 4.847	1.4 13	5.4 45	0.0 00	4.8 47	-93.22	0.0 379	1.640	2.71
TNM/N2 H4 (O/F = 1.40)	C0.298H5.181N 3.784O2.388	0.2 98	5.1 81	3.7 84	2.3 88	18.38	0.0 438	1.586	2.85
H2 O2 (90%)/N2 H4 (O/F = 1.50)	H8.836N2.497O 3.509	0.0 00	2.4 97	2.4 97	3.5 09	-79.15	0.0 522	1.335	2.70
RFNA- DETA/MA (80/20) (O/F = 3.00)	C0.936H4.491N 1.971O3.539	0.9 36	4.4 91	1.9 71	3.5 39	-54.24	0.0 388	1.364	2.61
RFNA/Hydine (O/F = 3.17)	C0.852H4.312N 2.004O3.587	0.8 52	4.3 12	2.0 04	3.5 87	-48.55	0.0 387	1.433	2.65

N2 O4 /N2 H4 (O/F = 1.30)	H5.418N3.940O 2.461	0.0 00	5.4 18	3.9 40	2.4 61	13.52	0.0 456	1.584	2.87
N2 O4 /Aerozine- 50 (O/F = 2.00)	C0.555H4.299N 3.044O2.900	0.5 55	4.2 99	3.0 44	2.9 00	6.32	0.0 405	1.658	2.83
N2 O4 /NO (70/30)-MeOH (O/F = 2.10)	C1.005H4.020N 1.710O3.746	1.0 05	4.0 20	1.7 10	3.7 46	-45.03	0.0 373	1.528	2.67
N2 O4 /NO (70/30)-NH3 (O/F = 2.10)	H5.672N3.601O 2.741	0.0 00	5.6 72	3.6 01	2.7 41	-20.17	0.0 459	1.393	2.73
O2 /HTPB (O/F = 2.30)	C2.144H3.227N 0.019O4.424	2.1 44	3.2 27	0.0 19	4.4 24	-10.91	0.0 303	2.144	2.91
H2 O2 (90%)/PE (O/F = 7.80)	C0.814H7.302O 5.181	0.8 14	7.3 02	0.0 00	5.1 81	- 144.4 3	0.0 442	1.385	2.63
H2 O2 (98%)/PE (O/F = 7.00)	C0.893H7.023O 5.140	0.8 93	7.0 23	0.0 00	5.1 40	- 125.5 3	0.0 433	1.540	2.71
H2 O2 (98%)/DCPD (O/F = 6.20)	C1.051H6.415O 5.058	1.0 51	6.4 15	0.0 00	5.0 58	- 112.3 7	0.0 413	1.600	2.70
H2 O2 (86%)/HTPB (O/F = 7.50)	C0.842H7.093N 0.007O5.167	0.8 42	7.0 93	0.0 07	5.1 67	- 117.8 9	0.0 436	1.633	2.76
H2 O2 (92%)/HTPB (O/F = 6.50)	C0.941H6.877N 0.008O5.105	0.9 41	6.8 77	0.0 08	5.1 05	- 116.2 4	0.0 428	1.609	2.75
RFNA/HTPB (O/F = 4.90)	C1.196H3.092N 1.371O3.959	1.1 96	3.0 92	1.3 71	3.9 59	-57.08	0.0 344	1.457	2.54
N2\O/Paraffin wax (O/F = 7.00)	C0.890H1.816N 3.976O1.988	0.8 90	1.8 19	3.9 76	1.9 88	32.64	0.0 344	1.359	2.60
N2 O/HTPB (O/F = 7.40)	C0.842H1.267N 4.011O2.028	0.8 42	1.2 67	4.0 11	2.0 28	37.38	0.0 334	1.396	2.61
HAN(95%)/HTP B (O/F = 9.60)	C0.665H5.089N 1.798O3.857	0.6 65	5.0 89	1.7 98	3.8 57	-89.89	0.0 410	1.189	2.49

REFERENCES

- [1] Chaturvedi, S., and Dave, P. N. Solid Propellants: AP/HTPB Composite Propellants. *Arabian Journal of Chemistry*. 8. Volume 12, 2061–2068.
- [2] DAINES, W., and BOYD, D. Effect of Aluminum Concentration in Propellant on Performance of Rocket Motors. 1976.
- [3] DAINES, W., BOARDMAN, T., LUND, R. K., and ABEL, R. Effect of Aluminum Oxide Impingement on Specific Impulse of Solid Propellant Rocket Motors. 1975.
- [4] Davis, D. K., and Abel, R. EFFECTS OF INTERNAL NOZZLE CONTOURING ON NOZZLE PERFORMANCE. 1983.
- [5] SMITH-KENT, R., RIDDER, J., LOH, H.-T., and ABEL, R. Effect of ITE and Nozzle Exit Cone Erosion on Specific Impulse of Solid Rocket Motors. 1993.
- [6] McBride, B. J., Gordon, S., and Cleveland, A. *NASA Reference Computer Program for Calculation of Complex Chemical Equilibrium Compositions and Applications II. Users Manual and Program Description*. 1311.
- [7] *Advanced Energetic Materials*. National Academies Press, Washington, D.C., 2004.
- [8] Becker, C. A., and Warren, J. A. Progress in Materials Data Availability and Application: A Review. *IEEE Signal Processing Magazine*. 1. Volume 39, 104–108.
- [9] Ward, C. H., Warren, J. A., and Hanisch, R. J. Making Materials Science and Engineering Data More Valuable Research Products. *Integrating Materials and Manufacturing Innovation*. 1. Volume 3, 292–308.
- [10] Medina-Smith, A., Becker, C. A., Plante, R. L., Bartolo, L. M., Dima, A., Warren, J. A., and Hanisch, R. J. “A Controlled Vocabulary and Metadata Schema for Materials Science Data Discovery.” *Data Science Journal*, Vol. 20, No. 18, 2021, pp. 1–10. <https://doi.org/10.5334/dsj>.

- [11] Owen, D. B., Mcrightt, P. S., and Cardiff+, E. H. *Implementation of an Online Database for Chemical Propulsion Systems*.
- [12] Verduzco, J. C., Marinero, E. E., and Strachan, A. “An Active Learning Approach for the Design of Doped LLZO Ceramic Garnets for Battery Applications.” *Integrating Materials and Manufacturing Innovation*, Vol. 10, No. 2, 2021, pp. 299–310. <https://doi.org/10.1007/s40192-021-00214-7>.
- [13] McClure, Z. D., and Strachan, A. “Expanding Materials Selection Via Transfer Learning for High-Temperature Oxide Selection.” *JOM*, Vol. 73, No. 1, 2021, pp. 103–115. <https://doi.org/10.1007/s11837-020-04411-1>.
- [14] Barnes, B. C., Elton, D. C., Boukouvalas, Z., Taylor, D. E., Mattson, W. D., Fuge, M. D., and Chung, P. W. *Machine Learning of Energetic Material Properties*.
- [15] Kamlet, M. J., and Jacobs, S. J. “Chemistry of Detonations. I. A Simple Method for Calculating Detonation Properties of C-H-N-O Explosives.” *The Journal of Chemical Physics*, Vol. 48, No. 1, 1968, pp. 23–35. <https://doi.org/10.1063/1.1667908>.
- [16] Frem, D. “A Reliable Method for Predicting the Specific Impulse of Chemical Propellants.” *Journal of Aerospace Technology and Management*, Vol. 10, 2018. <https://doi.org/10.5028/jatm.v10.945>.
- [17] Adam Shine. Basic Rocket Propulsion.
- [18] Tola, C., and Nikbay, M. Multidisciplinary Optimization of a Solid Propellant Sectional Geometry for Internal Ballistic and Structural Strength Criteria. 2016.
- [19] Devenport, W. J. Nozzle Applet. <https://www.engapplets.vt.edu/fluids/CDnozzle/cdinfo.html>.
- [20] Prianto, B., Setyaningsih, H., and Puspitasari, R. R. Analysis of Composite Propellant Energy and Correlation with Specific Impulse at Vacuum Level. No. 2226, 2020.

- [21] George, D. "RECENT ADVANCES IN SOLID ROCKET MOTOR PERFORMANCE PREDICTION CAPABILITY." *AIAA Paper*, 1981. <https://doi.org/10.2514/6.1981-33>.
- [22] Coats, D. E., and Dang, A. L. Improvements to the Solid Performance Program (SPP'12) and a Review of Nozzle Performance Predictions. 2014.
- [23] Stephen, W. A. *BALLISTIC MISSILE PROPELLANT EVALUATION TEST MOTOR SYSTEM (SUPER BATES)*. 1974.
- [24] "History of the BATES Motor."
- [25] Geisler, R. L., Enterprises, G., and Beckman, C. W. *The History of the BATES Motors at the Air Force Rocket Propulsion Laboratory*.
- [26] Stephenson, J. "Design of Nozzle for High-Powered Solid Rocket Propellant." *Undergraduate Journal of Mathematical Modeling: One + Two*, Vol. 9, No. 1, 2018. <https://doi.org/10.5038/2326-3652.9.1.4895>.
- [27] "Koch O138ThermochemicalCodes (1)."
- [28] Ho, T. K. Random Decision Forests. No. 1, 1995, pp. 278–282.
- [29] Pedregosa, F., Varoquaux, G., Gramfort, A., Michel V. and Thirion, B., Grisel, O., Blondel, M., Prettenhofer P. and Weiss, R., Dubourg, V., Vanderplas, J., Passos, A., Cournapeau, D., Brucher, M., Perrot, M., and Duchesnay, E. "Scikit-Learn: Machine Learning in Python." *Journal of Machine Learning Research*, Vol. 12, 2011, pp. 2825–2830.
- [30] Desai, S., and Strachan, A. "Parsimonious Neural Networks Learn Interpretable Physical Laws." *Scientific Reports*, Vol. 11, No. 1, 2021. <https://doi.org/10.1038/s41598-021-92278-w>.
- [31] Landsbaum, E. M., Salinas, M. P., and Leary, J. P. "Specific Impulse Prediction of Solid-Propellant Motors." *Journal of Spacecraft and Rockets*, Vol. 17, No. 5, 1980, pp. 400–406. <https://doi.org/10.2514/3.57758>.
- [32] Anderson, F. A., and West, W. R. *Altern-Ate Propellant Progra"m Phase [Final Report*.